

Targeted Gold Nanoparticles Enable Molecular CT Imaging of Cancer

Rachela Popovtzer,[†] Ashish Agrawal,[‡] Nicholas A. Kotov,[‡] Aron Popovtzer,[§]
James Balter,[§] Thomas. E. Carey,^{||} and Raoul Kopelman^{*†}

Department of Chemistry, University of Michigan, Ann Arbor, Michigan, Department of Chemical Engineering, University of Michigan, Ann Arbor, Michigan, Department of Radiation Oncology, University of Michigan, Ann Arbor, Michigan, Department of Otolaryngology/Head and Neck Surgery, University of Michigan, Ann Arbor, Michigan

Received September 24, 2008; Revised Manuscript Received October 23, 2008

ABSTRACT

X-ray based computed tomography (CT) is among the most convenient imaging/diagnostic tools in hospitals today in terms of availability, efficiency, and cost. However, in contrast to magnetic resonance imaging (MRI) and various nuclear medicine imaging modalities, CT is not considered a molecular imaging modality since targeted and molecularly specific contrast agents have not yet been developed. Here we describe a targeted molecular imaging platform that enables, for the first time, cancer detection at the cellular and molecular level with standard clinical CT. The method is based on gold nanoprobables that selectively and sensitively target tumor selective antigens while inducing distinct contrast in CT imaging (increased X-ray attenuation). We present an in vitro proof of principle demonstration for head and neck cancer, showing that the attenuation coefficient for the molecularly targeted cells is over 5 times higher than for identical but untargeted cancer cells or for normal cells. We expect this novel imaging tool to lead to significant improvements in cancer therapy due to earlier detection, accurate staging, and microtumor identification.

Imaging plays a critical role in overall cancer management: in diagnostics, staging, radiation planning, and evaluation of treatment efficiency. Standard clinical imaging modalities such as CT, MRI, and ultrasound can be categorized as structural imaging modalities; they are able to identify anatomical patterns and to provide basic information regarding tumor location, size, and spread based on endogenous contrast. However, these imaging modalities are not efficient in detecting tumors and metastases that are smaller than 0.5 cm and they can barely distinguish between benign and cancerous tumors.¹

Molecular imaging is an emerging field that integrates molecular biology with in vivo imaging in order to gain information regarding biological processes and to identify diseases based on molecular markers, which usually appear before the clinical presentation of the disease. Currently, positron emission tomography and single photon emission tomography are the main molecular imaging modalities in clinical use, however, they provide only functional information regarding molecular processes and metabolites, which is indirect and nonspecific to distinct cells or diseases.^{2,3}

Recently, various types of targeted nanoprobables have been developed for optical and MRI molecular imaging such as superparamagnetic nanoparticles,⁴⁻⁷ quantum dots,⁸⁻¹⁰ and gold nanoparticles as cancer optical imaging probes.¹¹⁻¹³

CT is one of the most useful diagnostic tools in hospitals today in terms of availability, efficiency, and cost. Currently, CT is not a molecular imaging modality since relevant targeted and molecularly specific contrast agents have not yet been developed. Present CT contrast agents are predominantly based on iodine containing molecules, which are effective in absorbing X-rays; however, they are nonspecifically targeted because they cannot be conjugated to most biological components or cancer markers and they allow only very short imaging times due to rapid clearance by the kidneys.

Gold induces a strong X-ray attenuation, as was first demonstrated, inadvertently, by Wilhelm Roentgen, in the first X-ray human image (Figure 1). Gold nanoparticles have, in addition, unique physical, chemical, and biological properties, which make them an ideal candidate for CT contrast agents. The ability of CT to distinguish between different tissues is based on the fact that different tissues provide different degrees of X-ray attenuation, where the attenuation coefficient is determined by the atomic number and electron density of the tissue; the higher the atomic number and electron density, the higher the attenuation coefficient. The atomic number and electron density of gold (79 and 19.32 g/cm³, respectively) are much higher than those of the

* Corresponding author. E-mail: kopelman@umich.edu. Phone: 734-764-7541. Fax: 734-936-2778.

[†] Department of Chemistry, University of Michigan.

[‡] Department of Chemical Engineering, University of Michigan.

[§] Department of Radiation Oncology, University of Michigan.

^{||} Department of Otolaryngology/Head and Neck Surgery, University of Michigan.



Figure 1. First ever medical X-ray image (1895) taken by Roentgen. “Hand with Ring” print of Wilhelm Roentgen’s first “medical” X-ray, taken on 22 December 1895. It dramatically showed the bones of her fingers; however the real size of her finger’s soft tissue could be garnered from the clearly visible gold ring on her finger. Likewise, below we show that “ringing” the tumor cells with gold nanoparticles makes it effectively more visible to CT. Note that the size of the ring maps the width of the finger’s soft tissue. Radiology Centennial, Inc. copyrighted in 1993.

currently used iodine (53 and 4.9 g/cm³). Note that for CT imaging, the total amount of gold per unit volume (voxel) is the only important parameter regardless of the shape of the particles. In addition, gold nanoparticles provide a high degree of flexibility in terms of functional groups for coating and targeting and have also proved to be nontoxic and biocompatible *in vivo*.^{14,15}

Recent progress toward nanotechnology based CT imaging has been made by Hainfeld et al.;¹⁶ they demonstrated the feasibility of gold nanoparticles to induce *in vivo* vascular contrast enhancement in CT imaging, however the gold particles were not targeted as they were not conjugated to specific biomarkers. More recently, hybrid nanoparticles such as antibiofouling polymer-coated gold nanoparticles,^{17,18} gadolinium-coated gold nanoparticles,¹⁹ PEG-coated nanoparticles,²⁰ and polymer-coated Bi₂S₃ nanoparticles²¹ have been developed as vascular CT contrast agents.

In this study, we describe a new platform for *in vivo* CT molecular imaging based on new class of immuno-targeted gold nanoprobe that selectively and sensitively target tumor specific antigens. These gold nanoprobe form a concentrated assembly on the cancer cells, yielding a distinguishable X-ray attenuation, which is not typical for nondecorated cells or tissue. This transforms the targeted cancer into highly distinct and easy to diagnose features.

While a CT molecular imaging agent would potentially have broad applicability for many cancer types, for this research we have chosen to work with head and neck cancer, which is the fifth most common cancer worldwide.²² Squamous cell carcinoma (SCC) represents more than 90% of all head and neck cancers. Many SCC of the head and neck present as advanced tumors for which the true extent is difficult to determine from present CT and physical examination. Cure rates for oral cancers have declined²³ in recent

years, and better diagnostic tools are needed for accurate staging and discovery of tumor extent. Previously it has been demonstrated that SCC is characterized by significant over-expression of the A9 antigen,²⁴ which is also called the $\alpha 6 \beta 4$ integrin,²⁵ and that there is a strong correlation between the A9 expression level and metastatic behavior.²⁶ It has also been demonstrated that the UM-A9 antibody can home onto SCC tumors *in vivo*.²⁷ An additional reason for choosing head and neck cancer was because one of its major diagnostic challenges today is a reliable detection of involved lymph nodes because their status is one of the most important prognosis predictors and is also critical for appropriate treatment. However, assessment of lymph nodes based on structural imaging features is limited in sensitivity and specificity and fails to distinguish between non-neoplastic and malignant processes. These limitations lead to the routine performance of prophylactic procedures such as extensive neck dissection and radiation and, on the other hand, a lack of treatment for undiagnosed small metastases, which is the first cause of the reappearance of cancer. Hence, the development of more sensitive *in vivo* imaging techniques is of major importance and could substantially improve head and neck cancer diagnosis, treatment, and potential cure.

In these experiments, we synthesized gold nanorods (AuNR) and conjugated them with UM-A9 antibodies, which home specifically to SCC head and neck cancer.²⁷ We examined their feasibility to effectively induce contrast enhancement in CT imaging, as a specific and sensitive targeted probe in head and neck cancer. Note that for CT imaging the total amount of gold per unit volume (voxel) is the only important parameter, regardless the shape of the particles. AuNR are more advantageous in comparison with spherical nanoparticles because they offer a complementary method of detection for some cancers based on their IR adsorption.^{28,29} Most importantly, in comparison with other techniques utilizing optical properties of AuNR, CT scans are not limited by the depth of cancer in the tissue.

Gold nanorods fabrication: AuNR were synthesized using the seed mediated growth method.³⁰ The mean length was 45 nm and the mean diameter was 15 nm with gold concentration of 2.5 mg/mL. **Antibody conjugation:** The bioconjugation of the AuNR to the UM-A9 antibody was achieved according to the method described by Kim et al.³¹ Briefly, a layer of biocompatible^{32–34} poly(acrylic acid) (PAA) was adsorbed onto the surface of gold nanorods followed by addition of EDC/NHS. PAA-coated nanorods were dispersed in 1 mL of PBS (pH 6.0) buffer, followed by 100 μ L (*N*-ethyl-*N'*-(3-dimethylaminopropyl)carbodiimide) EDC and 100 μ L of 0.2 M (*N*-hydroxy-succinimide) NHS mixture to provide active sites on gold nanorods that undergo amidation reaction with the antibodies. The amount of antibody added is 20 μ g per 1.96 mg of molecular gold. The mixture was stored overnight in refrigerator at 4 °C, followed by centrifugation and redispersion in ultrapure water to remove unbound antibody in the solution.

Cell culture: UM-SCC-1 and UM-SCC-5 human head and neck cancer cell lines and the negative control samples of fibrosarcoma (UM-FS-1) and melanoma (UM-Mel-1), which

are known not to express the A9 antigen, were cultured in DMEM media supplemented with 10% fetal bovine serum, 1 mM sodium pyruvate, 100 units/mL penicillin, 100 $\mu\text{g}/\text{mL}$ streptomycin sulfate, and 292 $\mu\text{g}/\text{mL}$ L-glutamine (all from InVitrogen, Carlsbad CA).

Cells-AuNR binding: One milliliter of cell suspension (10^6 cells/mL) was mixed with 1 mL of antibody-coated AuNR solution (2.5 mg/mL) and allowed to interact for 90 min at room temperature. Then, the solution was 3 times centrifuged at 1000 rpm for 5 min to wash out unbound antibody from the AuNR-antibody complexes; after each centrifugation step, the mixture was redispersed in PBS solution (1 mL total volume).

CT scans: all scans were performed using clinical CT at 80 kVp (GE Lightspeed QX/I; General Electric, Waukesha, WI). The suspensions, in cuvettes, were scanned using a shaped Styrofoam assembly to hold the samples in place.

CT Imaging Experiment. Two SCC human head and neck cancer cell lines (10^6 cells/mL) were used; oral cancer UM-SCC-1 and larynx cancer UM-SCC-5. Both cancerous cell lines were shown before to have a significant overexpression of the A9 antigen.²⁴ CT imaging was performed on the SCC cells, which were targeted with the UM-A9 antibody-coated gold nanorods.

The following negative control experiments were performed: (a) CT imaging of the same head and neck cancer cells (UM-SCC-1 and UM-SCC-5) in a suspension, without the addition of nanoparticles, (b) CT imaging of the same head and neck cancer cells that were targeted with gold nanorods that were coated with antibodies that *do not match* with the SCC cells (*KHRI-3*), and (c) CT imaging of noncancerous cells (normal fibroblast cells) and of other types of cancer cells (melanoma) that were targeted with the UM-A9 antibodies-coated gold nanorods. CT imaging of a solution of bare gold nanorods (suspended in water, without any cells) provides the positive control.

The attenuation values (HU) that were obtained from the CT imaging are shown in Figure 2.

As shown in Figure 2, the change in the *attenuation coefficient* (with respect to water) of the SCC cancer cells that were targeted by the A9 antibody-coated gold nanorods is over 5 times higher than that of the nontargeted SCC cancer cells (32 and 28 HU vs 168 and 172 HU, respectively). This demonstrates that the gold nanorods were attached to the cancer cells with high density, yielding a distinguishable CT attenuation number that is higher than that for typical soft tissue (typical attenuation values for solid tissue are in the range of 0–50 HU), thus making the targeted cells detectable in sufficient concentration. The attenuation values observed for the negative control samples that were targeted with gold nanorods (larynx and oral cancer cells targeted with nanorods that are coated with nonmatching antibodies and normal fibroblast and melanoma cells targeted with A9 antibodies) revealed relatively low nonspecific binding (58, 54, 50, 62 HU, respectively) and demonstrate that head and neck tumors may show a likely enhancement of 3–4 times the local contrast of nontargeted tissue *in vivo*. Such a specificity and local enhancement is consistent with

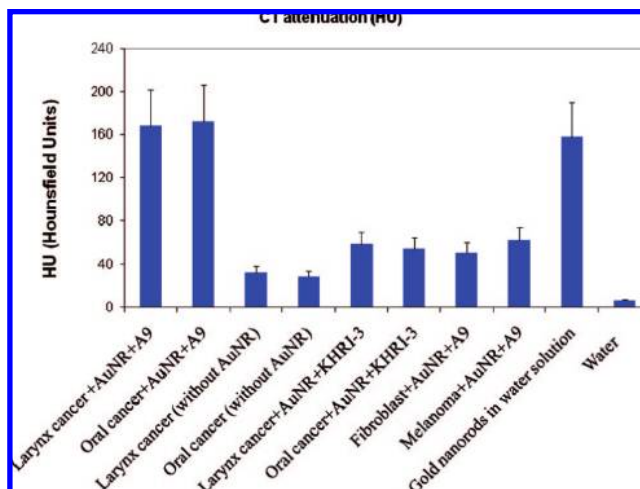


Figure 2. CT attenuation (HU) of SCC head and neck cancer cells and positive and negative control samples. Bar graph with standard deviation of 3 samples: larynx and oral cancer cells that were targeted with A9 antibody-coated gold nanorods (AuNR), larynx and oral cancer cells without gold nanorods, larynx and oral cancer cells targeted with nanorods that are coated with nonmatching antibodies (KHRI-3); normal fibroblast and melanoma cells targeted with A9 antibodies, bare gold nanorods in water solution (2.5 mg/mL), and water.

a previous study investigating the potential use of UM-A9 as a radiolabeled imaging agent for human squamous carcinoma tumors *in vivo*.²⁷ The attenuation value observed for the positive control sample, the bare gold nanorods, is 158 HU; this high number was expected because the sample contained a high concentration of gold (2.5 mg/mL).

In these experiments, we tested 1 mL samples that contained 10^6 SCC cancer cells. Assuming the size of one SCC cancer cell is approximately 10 μm , there may be sufficient differential signal from tumors as small as 1 mm^3 to provide detectable contrast, nearly at the limit of resolution for clinical CT scanning. Another important parameter that should be noted is the high differential contrasts that have been obtained in the above experiments. The signal (HU) obtained from the targeted SCC is significantly higher than the background value (defined as the HU obtained from the control experiments). The enhancement of local signal increases local CT attenuation above the normal values for soft tissue, thus providing encouraging initial indications that sufficient specificity can be obtained in *in vivo* experiments.

Light Scattering Images of Targeted and Nontargeted SCC Head and Neck Cancer Cells. SCC head and neck cancer cells that were targeted with UM-A9 antibody-coated gold nanorods and SCC that were incubated with nonmatching antibodies (R-KHRI-3) coated gold nanorods were placed on a slide for dark field microscope imaging. Figure 3 shows, for the scattering images, clearly distinguishable differences between the specifically and selectively targeted SCC cells and those that were exposed to nonmatching coated gold nanorods. The SCC cancer cells (oral and larynx cancer) that were targeted with the nonmatching antibody-coated gold nanorods yielded only a small amount of scattered light, resulting from the nonspecific binding. Yet, these images clearly illustrate that only

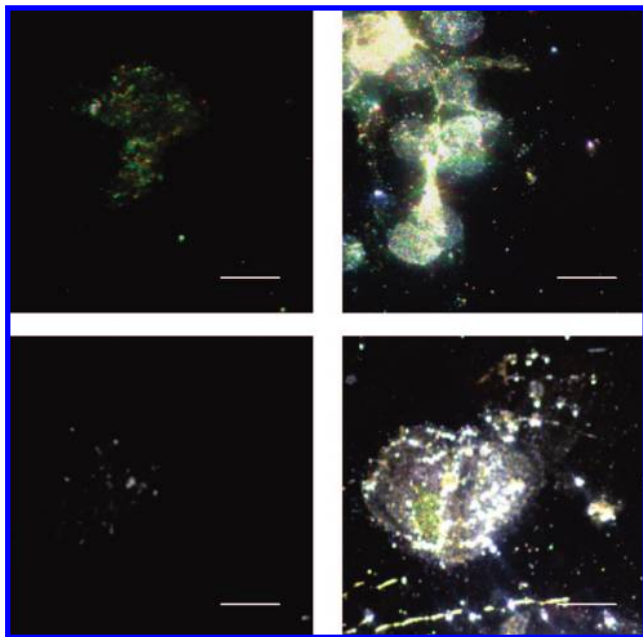


Figure 3. Dark field microscope images of SCC head and neck cancer cells. Dark field microscope images of SCC head and neck cancer cells (oral cancer upper images, larynx cancer lower images) after incubation with nonmatching antibody-coated gold nanorods (left) vs matching UM-A9 antibody-coated gold nanorods (right). Scale bar: 10 μm .

the correctly conjugated nanoparticles bind specifically, with high concentrations, to the surfaces of the SCC cells.

In conclusion, these proof of principle experiments demonstrated that we may be able to identify, through CT scans, the existence of SCC cancer cells; the concentrated assembly of gold nanoparticles that form exclusively on the targeted cancer cells yield a strong selective X-ray attenuation that is distinct from the attenuation obtained by identical but untargeted cancer cells or by normal cells.

We expect that the CT molecular imaging technique will revolutionize modern head and neck cancer diagnosis and staging, by allowing reliable and sensitive detection of lymph nodes and other metastasis, which are not available today. This might also prevent or minimize the now routinely performed neck dissection, which is associated with considerable morbidity. The importance of such a technique is further reinforced because of the vast availability and the extensive use of CT in clinics today and will provide the ability to perform simultaneously macroscopic (CT) and microscopic (molecular based CT) imaging.

Acknowledgment. This work was supported by the CRC-UM grant, UM Head and Neck Cancer SPORE NCI/NIDCR P50 CA97248, the National Science Foundation BioSensor Program, NSF-DMR 0455330 (RK), and AFOSR under MURI grant FA9550-06-1-0337.

References

(1) Rusinek, H.; Naidich, D. P.; McGuinness, G.; Leitman, B. S.; McCauley, D. I.; Krinsky, G. A.; Clayton, K.; Cohen, H. *Radiology* **1998**, *209*, 243–249.

(2) Al-Nahha, A.; Win, Z.; Szyszko, T.; Singh, A.; Nanni, C.; Fanti, S.; Rubello, D. *Anticancer Res.* **2007**, *27*, 4087–4094.

(3) Nanni, C.; Rubello, D.; Fanti, S.; Farsad, M.; Ambrosini, V.; Rampin, L.; Banti, E.; Carpi, A.; Muzzio, P.; Franchi, R. *Biomed. Pharmacother.* **2006**, *60*, 409–413.

(4) Lamerichs, R. *Cell. Oncol.* **2008**, *30*, 100–100.

(5) Sun, C.; Veisoh, O.; Gunn, J.; Fang, C.; Hansen, S.; Lee, D.; Sze, R.; Ellenbogen, R. G.; Olson, J.; Zhang, M. *Small* **2008**, *4*, 372–379.

(6) Kopelman, R.; Koo, Y.-E. L.; Philbert, M.; Moffat, B. A.; Reddy, G. R.; McConville, P.; Hall, D. E.; Chenevert, T. L.; Bhojani, M. S.; Buck, S. M.; Rehemtulla, A.; Ross, B. D. *J. Magn. Magn. Mater.* **2005**, *293*, 404–410.

(7) Koo, Y. E. L.; Reddy, G. R.; Bhojani, M.; Schneider, R.; Philbert, M. A.; Rehemtulla, A.; Ross, B. D.; Kopelman, R. *Adv. Drug Delivery Rev.* **2006**, *58*, 1556–1577.

(8) Gao, X. H.; Nie, S. M. *Nanosensing: Mater. Devices* **2004**, *5593*, 292–299.

(9) Diagaradjane, P.; Orenstein-Cardona, J. M.; Colón-Casasnovas, N. E.; Deorukhkar, A.; Shentu, S.; Kuno, N.; Schwartz, D. L.; Gelovani, J. G.; Krishnan, S. *Clin. Cancer Res.* **2008**, *14*, 731–741.

(10) Guo, Y.; Shi, D.; Lian, J.; Dong, Z.; Wang, W.; Cho, H.; Liu, G.; Wang, L.; Ewing, R. C. *Nanotechnology* **2008**, *19*, 175102.

(11) Huang, X. H.; El-Sayed, I. H.; Qian, W.; El-Sayed, M. A. *Nano Lett.* **2007**, *7*, 1591–1597.

(12) Jain, P. K.; El-Sayed, I. H.; El-Sayed, M. A. *Nano Today* **2007**, *2*, 18–29.

(13) Huang, X. H.; Jain, P. K.; El-Sayed, I. H.; El-Sayed, M. A. *Nanomedicine* **2007**, *2*, 681–693.

(14) Connor, E. E.; Mwamuka, J.; Gole, A.; Murphy, C. J.; Wyatt, M. D. *Small* **2005**, *1*, 325–327.

(15) Hauck, T. S.; Ghazani, A. A.; Chan, W. C. W. *Small* **2008**, *4*, 153–159.

(16) Hainfeld, J. F.; Slatkin, D. N.; Focella, T. M.; Smilowitz, H. M. *Br. J. Radiol.* **2006**, *79*, 248–253.

(17) Kim, D.; Park, S.; Lee, J. H.; Jeong, Y. Y.; Jon, S. *J. Am. Chem. Soc.* **2007**, *129*, 7661–7665.

(18) Kattumuri, V.; Katti, K.; Bhaskaran, S.; Boote, E. J.; Casteel, S. W.; Fent, G. M.; Robertson, D. J.; Chandrasekhar, M.; Kannan, R.; Katti, K. V. *Small* **2007**, *3*, 333–341.

(19) Alric, C.; Taleb, J.; Le Duc, G.; Mandon, C.; Billotey, C.; Le Meur-Herland, A.; Brochard, T.; Vocanson, F.; Janier, M.; Perriat, P.; Roux, S.; Tillement, O. *J. Am. Chem. Soc.* **2008**, *130*, 5908–5915.

(20) Cai, Q. Y.; Kim, S. H.; Choi, K. S.; Kim, S. Y.; Byun, S. J.; Kim, K. W.; Park, S. H.; Juhng, S. K.; Yoon, K. H. *Invest. Radiol.* **2007**, *42*, 797–806.

(21) Rabin, O.; Perez, J. M.; Grimm, J.; Wojtkiewicz, G.; Weissleder, R. *Nat. Mater.* **2006**, *5*, 118–122.

(22) Chin, D.; Boyle, G. M.; Porceddu, S.; Theile, D. R.; Parsons, P. G.; Coman, W. B. *Expert Rev. Anticancer Ther.* **2006**, *6*, 1111–1118.

(23) Carvalho, A. L.; Nishimoto, I. N.; Califano, J. A.; Kowalski, L. P. *Int. J. Cancer* **2005**, *114*, 806–816.

(24) Kimmel, K. A.; Carey, T. E. *Cancer Res.* **1986**, *46*, 3614–3623.

(25) Van Waes, C.; Kozarsky, K. F.; Warren, A. B.; Kidd, L.; Paugh, D.; Liebert, M.; Carey, T. E. *Cancer Res.* **1991**, *51*, 2395–2402.

(26) Wolf, G. T.; Carey, T. E.; Schmaltz, S. P.; McClatchey, K. D.; Poore, J.; Glaser, L.; Hayashida, D. J. S.; Hsu, S. *J. Natl. Cancer Inst.* **1990**, *82*, 1566–1572.

(27) Wahl, R. L.; Kimmel, K. A.; Beierwaltes, W. H.; Carey, T. E. *Hybridoma* **1987**, *6*, 111–119.

(28) Huang, X. H.; El-Sayed, I. H.; Qian, W.; El-Sayed, M. A. *J. Am. Chem. Soc.* **2006**, *128*, 2115–2120.

(29) Gobin, A. M.; Lee, M. H.; Halas, N. J.; James, W. D.; Drezek, R. A.; West, J. L. *Nano Lett.* **2007**, *7*, 1929–1934.

(30) Nikoobakht, B.; El-Sayed, M. A. *Chem. Mater.* **2003**, *15*, 1957–1962.

(31) Kim, K.; Huang, S.-W.; Ashkenazi, S.; O'Donnell, M.; Agarwal, A.; Kotov, N. A.; Denny, M. F.; Kaplan, M. *Appl. Phys. Lett.* **2007**, *90*, 223901.

(32) Chamberland, D. L.; Agarwal, A.; Kotov, N.; Fowlkes, J. B.; Carson, P. L.; Wang, X. *Nanotechnology* **2008**, *19*, 095101.

(33) Yoshida, M.; Roh, K. H.; Lahann, J. *Biomaterials* **2007**, *28*, 2446–2456.

(34) Agarwal, A.; Huang, S. W.; O'Donnell, M.; Day, K. C.; Day, M.; Kotov, N.; Ashkenazi, S. *J. Appl. Phys.* **2007**, *102*, 064701.

NL8029114